Navarro-Jiménez, J.; Nadal, E.; Tur Valiente, M.; Martínez Casas, J.; Ródenas, JJ. (2020). On the use of stabilization techniques in the Cartesian grid finite element method framework for iterative solvers. International Journal for Numerical Methods in Engineering. 121(13):3004-3020. https://doi.org/10.1002/nme.6344

On the use of stabilization techniques in the cgFEM framework for iterative solvers

José Manuel Navarro-Jiménez[1], Enrique Nadal[1], Manuel Tur[1], José Martínez-Casas[1], Juan José Ródenas[1,2]

[1] Centro de Investigación en Ingeniería Mecánica (CIIM)
Universitat Politècnica de València, Camino de Vera s/n, 46071 Valencia, Spain
jonaji@upv.es, ennaso@upvnet.upv.es, {matuva, jomarc12, jjrodena}@mcm.upv.es

[2] Healthcare Technology Group (GTS-IBV)
Networking Biomedical Research Centre in Bioengineering, Biomaterials and Nanomedicine (CIBER-BBN)
Universitat Politècnica de València, Spain

Abstract

Fictitious Domain Methods, like the Cartesian grid Finite Element Method (cgFEM), are based on the use of unfitted meshes that must be intersected. This may yield to ill-conditioned systems of equations since the stiffness associated with a node could be small, thus poorly contributing to the energy of the problem. This issue complicates the use of iterative solvers for large problems. In this work, we present a new stabilization technique that, in the case of cgFEM, preserves the Cartesian structure of the mesh. The formulation consists in penalizing the free movement of those nodes by a smooth extension of the solution from the interior of the domain, through a post-process of the solution via a displacement recovery technique. The numerical results show an improvement of the condition number and a decrease in the number of iterations of the iterative solver while preserving the problem accuracy.

Keywords: cgFEM, Iterative Solver, Fictitious Domain, Condition number

1 Introduction

During the last decades of the XX^{th} century, a parallel concept to the Finite Element Method (FEM) emerged, the Fictitious Domain Method (FDM). According to [1], a wide amount of variants have been developed since V.K. Saul'ev published, in Russian, the paper *Solution of certain boundary-value problems on high-speed computers by the fictitious-domain method* (Sibirsk. Mat.Z. 1963.4:912-925). In the FEM framework, the geometry of the component to be analyzed is conformingly meshed. Therefore, the mesh generation complexity is directly related to the complexity of the geometry. Besides the existence of advanced and automated mesh generators algorithms [2, 3], the meshing process is one of the most tedious processes during the FE analysis. On the contrary, the FDM is based on embedding the problem domain into a fictitious domain, i.e. a square in 2D or a cube in 3D, which is easy to mesh. The FDM completely separates the mesh used for solving the Finite Element (FE) problem from the geometry of the component. Therefore the component's geometry is not related to the mesh generation process, which is usually octree-based. Since the FE mesh is not related to the geometry, special treatment of the geometry is needed in the FDM. This important issue is usually the key ingredient that distinguishes the different approaches of the FDM.

Recently the FDM has gained additional interest since problems without CAD geometry are arising in numerical simulations. This sort of problems embraces, among others, those coming from medical images. In that sense, the Finite Cell Method [4, 5] and the Cartesian grid Finite Element Method (cgFEM) [6, 7] have demonstrated their capabilities to deal with these problems [8, 9].

Independently of the approach used, most of these methods face difficulties in similar aspects: imposing the Dirichlet boundary conditions, numerical conditioning, accuracy over the boundary, etc. In this sense, the FDM so-called CutFEM [10] proposes a robust methodology to guarantee problem well-posedness and the proper imposition of the Dirichlet boundary conditions. cgFEM [11, 12] also uses stabilization methods based on smoothed stress fields for imposing Dirichlet boundary conditions guaranteeing the coercivity of the problem. These stabilization procedures can guarantee the solvability of the problem at hand for direct solvers.

However, when iterative solvers are needed, not only solvability must be guaranteed but also that the condition number of the system of equations is under control to improve the performance of the iterative solver. In that sense, the use of standard preconditioners (those prepared for body-fitted meshes) is not adequate in this context. Recently, some preconditioners have been developed for FDMs but they are mainly serial non-scalable algorithms [13, 14, 15]. The other approach is to focus on the kernel of the problem, which is the badly cut cells. Since in the FDM framework the elements are intersected by the geometry, there are situations in which the nodes are far from the boundary, having a small influence on the energy of the solution, as you can appreciate in Figure 1. In other words, the value of the solution at these nodes is not relevant in the minimization of the potential energy, therefore elevating the condition number of the system of equations. A common approach is to use a small stiffness in the embedding domain [16], or to exclude the assembly of the elements with small support [17, 18]. More advanced techniques, like the Ghost Penalty Method [19], have been implemented in CutFEM. Badía *et. al.* [20] implemented a technique that uses aggregates (macro-elements formed by joining together contiguous elements) to increase the stiffness associated with nodes outside the problem domain. More recently Jomo *et. al.* [21] proposed the use of preconditioners for the Finite Cell Method in the context of iterative solvers. In this paper we propose a technique to keep under control the solution at these nodes while keeping the right convergence rate and accuracy of the solution. This will allow us to efficiently use iterative solvers for large problems in the FDM framework.

This paper is structured as follows: after this introduction, the problem model and the formulation of the proposed stabilization terms are introduced in Section 2. Section 3 is devoted to recalling the recovery procedures used for the stabilization terms and Section 4 contains a convergence analysis of the proposed stabilization terms. Section 5 illustrates the numerical resolution algorithm. Finally, the numerical results and conclusions are in Sections 6 and 7, respectively.

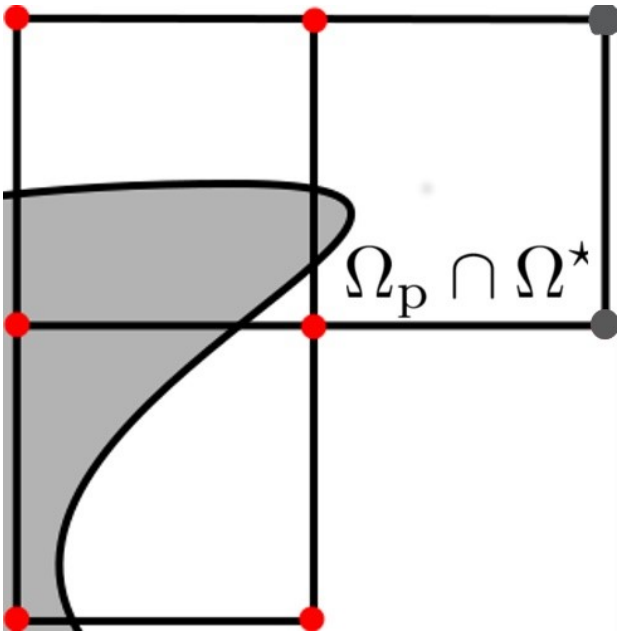

Figure 1: Ill-conditioning issue due to the mesh-geometry intersection. Grey nodes may cause ill-conditioning issues. $\Omega^\star$ corresponds to the domain of the mesh and Ω_p is the domain of the element with a grey node.

2 Problem statement

This paper is devoted to solving the 3D linear elasticity problem utilizing the cgFEM. The notation used all along the contribution is settled in this Section. The Cauchy stress field is denoted as $\boldsymbol{\sigma}$, the displacement field as $\mathbf{u}$, and the strain field as $\boldsymbol{\varepsilon}$, all these fields being defined over the domain $\Omega \subset \mathbb{R}^3$, with boundary denoted by $\partial\Omega$. Prescribed tractions denoted by $\mathbf{t}$ are imposed over the part Γ_N of the boundary, while displacements denoted by $\bar{\mathbf{u}}$ are prescribed over the complementary part Γ_D of the boundary. Body loads are denoted as $\mathbf{b}$.

The linear elasticity problem takes the primal variational form:

$$\begin{aligned} &\text{Find } \mathbf{u} \in (V_\Omega + \{\mathbf{w}\}) : \forall \mathbf{v} \in V_\Omega \\ &a(\mathbf{u},\mathbf{v})_\Omega = l(\mathbf{v})_\Omega \qquad \text{where} \\ &a(\mathbf{u},\mathbf{v})_\Omega = \int_\Omega \boldsymbol{\varepsilon}(\mathbf{u}) : \boldsymbol{\sigma}(\mathbf{v})\, \mathrm{d}\Omega \\ &l(\mathbf{v})_\Omega = \int_\Omega \mathbf{b}\cdot\mathbf{v}\, \mathrm{d}\Omega + \int_{\Gamma_N} \mathbf{t}\cdot\mathbf{v}\, \mathrm{d}\Gamma, \end{aligned} \tag{1}$$

where $V_\Omega = \{\mathbf{v} \mid \mathbf{v} \in [H^1(\Omega)]^3, \mathbf{v}|_{\Gamma_D} = \mathbf{0}\}$, $\mathbf{w}$ is a particular displacement field satisfying the Dirichlet boundary conditions and $\boldsymbol{\sigma}(\mathbf{v}) = \mathbf{D} : \boldsymbol{\varepsilon}(\mathbf{v})$, being $\mathbf{D}$ the fourth-order tensor relating the stress tensor with the strain tensor, defined as the symmetric gradient of the displacement field. Equation (1) settles the linear elasticity problem for the standard FEM. However, in the cgFEM framework an additional domain, $\Omega^\star$, embedding Ω as shown in Figure 2, should be introduced.

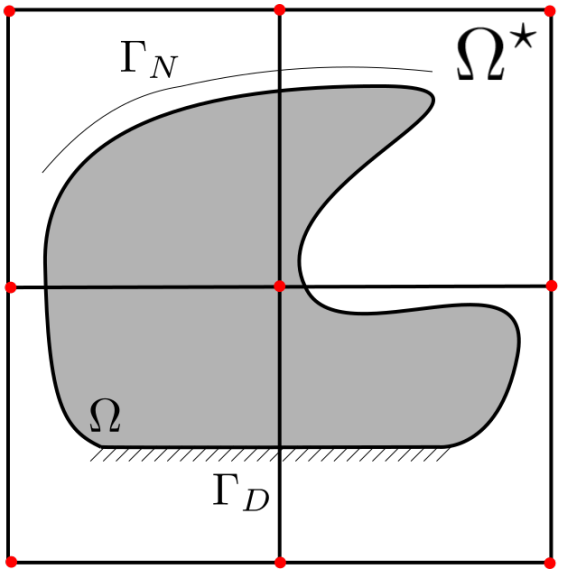

Figure 2: Representation of a problem domain Ω and the embedding domain $\Omega^\star$ in the cgFEM framework.

This modification of the problem domain leads to a formal modification of the problem (1) in the

following way:

$$\begin{aligned}
&\text{Find } \mathbf{u} \in (V_0 + \{\mathbf{w}\}) : \forall \mathbf{v} \in V_0 \\
&a(\mathbf{u}, \mathbf{v}) = l(\mathbf{v}) \qquad \text{where} \\
&a(\mathbf{u}, \mathbf{v}) = \int_{\Omega^\star} \boldsymbol{\varepsilon}(\mathbf{u}) : \boldsymbol{\sigma}(\mathbf{v}) \, \mathrm{d}\Omega \\
&l(\mathbf{v}) = \int_{\Omega^\star} \mathbf{b} \cdot \mathbf{v} \, \mathrm{d}\Omega + \int_{\Gamma_N} \mathbf{t} \cdot \mathbf{v} \, \mathrm{d}\Gamma,
\end{aligned} \tag{2}$$

where $V_0 = \{\mathbf{v} \mid \mathbf{v} \in [H^1(\Omega^\star)]^3, \mathbf{v}|_{\Gamma_D} = \mathbf{0}\}$. Note that $a(\mathbf{u}, \mathbf{v}) = a(\mathbf{u}, \mathbf{v})_\Omega$ and $l(\mathbf{v}) = l(\mathbf{v})_\Omega$ since $\mathbf{D} \equiv 0$ and $\mathbf{b} \equiv 0$ outside the domain Ω.

2.1 Boundary conditions in cgFEM

When using the cgFEM for numerically solving the problem (2), we find out that the Dirichlet boundary conditions cannot be directly applied as in the standard FEM since, in general, there are not any nodes over the boundary, as in Figure 2. As problem (2) is a constrained optimization problem, the Lagrange Multipliers technique can be applied. To do that, a Lagrange multipliers discretization over the Dirichlet boundaries is needed. The choice of the Lagrange multipliers space is crucial for the appropriate behavior of the proposed method. In this sense, some authors [22, 23] proposed the Vital Vertex Method for the 2D case which, *a prioiri*, defines an appropriate discretization for the Lagrange multiplier space. However, the extension of this procedure to the 3D case is not trivial. One alternative to these methods is the use of stabilized methods such as the ones proposed by Hansbo *et. al.* [24] and Burman and Hansbo [25] which are an adaptation of the Nitsche's method to the FDM framework, using the element traction jumps for stabilization purposes. In the context of the Finite Cell Method, the authors propose the use of a Nitsche's based approach for imposing the essential boundary conditions [9]. More recently Tur *et. al.* [11] propose a stabilization technique that makes use of recovery procedures easing the implementation of the method, especially for the 3D case. This last method is adopted in this contribution. To impose the Dirichlet boundary conditions in a weak sense implies the use of Lagrange multipliers. Therefore, solving problem (2) is equivalent to find the saddle point $(\mathbf{u}, \boldsymbol{\lambda})$ of the following Lagrangian:

$$\mathscr{L}_0(\mathbf{w}, \boldsymbol{\chi}) = a(\mathbf{w}, \mathbf{w}) + b(\boldsymbol{\chi}^h, \mathbf{w}) - l(\mathbf{w}), \tag{3}$$

where Lagrange multipliers belongs to the Hilbert space, $\boldsymbol{\lambda}, \boldsymbol{\chi} \in M$, $M = \{H^{-\frac{1}{2}}(\Gamma_D)\}^3$, $\mathbf{w}$ belongs to $V = \{\mathbf{v} \mid \mathbf{v} \in [H^1(\Omega^\star)]^3\}$ and

$$b(\boldsymbol{\chi}, \mathbf{w}) = \int_{\Gamma_D} \boldsymbol{\chi}^h \cdot \mathbf{w}^h \, \mathrm{d}\Gamma. \tag{4}$$

Note that, in general, the appropriate Lagrange multipliers space is not easy to find since, in the discrete counterpart, it is problem-dependent and it also depends on the way the mesh and the geometry intersect. In this work, the approach first presented in [26], which introduces a Lagrange multiplier at each integration point of the surface defining a polynomial approximation (piece-wise discontinuous polynomial approximation), is followed. This discretization does not fulfill the Ladyzhenskaya-Babuška-Brezzi (LBB) condition in general, therefore an additional stabilization term is added:

$$\mathscr{L}_S(\mathbf{w}^h, \boldsymbol{\chi}^h) = \mathscr{L}_0(\mathbf{w}^h, \boldsymbol{\chi}^h) - \frac{h}{k_1} \int_{\Gamma_D} \boldsymbol{\chi}^h \cdot (\boldsymbol{\lambda}^h + \mathbf{T}(\tilde{\mathbf{u}}^h)) \, \mathrm{d}\Gamma, \tag{5}$$

where $\mathbf{w}^h \in V^h$, the discrete counterpart of V, $\boldsymbol{\chi}^h \in M^h$, the discrete counterpart of M, k_1 is a parameter defined by the user, h is the characteristic mesh size and $\mathbf{T}(\tilde{\mathbf{u}}^h)$ is a recovered traction field depending on the FE solution $\tilde{\mathbf{u}}^h$ computed in previous Richardson's iterations. Note that since the solution depends on the FE solution $\tilde{\mathbf{u}}^h$, Richardson's iterations will be used to solve the problem as described in Section 5. Further details can be found in [11].

Expression (5) is similar to the one used in the Nitsche's method in which the operator $\mathbf{T}(\tilde{\mathbf{u}}^h)$ is replaced by the tractions over the Dirichlet boundary ($\boldsymbol{\sigma}(\mathbf{u}^h)$). In the proposed approach, the operator $\mathbf{T}(\tilde{\mathbf{u}}^h)$ is a postprocess of the solution, guaranteeing the correct convergence of the method [11]. Further details about the evaluation of this operator are given in Section 3.1. Problem (5) is already solvable since essential boundary conditions are properly imposed, thanks to the proper stabilization of the Lagrange multipliers field.

However, the problem can become ill-conditioned depending on how the mesh and the geometry intersect. This is not an important issue for small problems since direct solvers can solve them without major difficulties. In the case of larger problems, iterative solvers are used. The convergence of the iterative solvers is strongly affected by the condition number of the system to solve [27]. In the case of FDM in general, and particularly in the case of cgFEM, there are some mesh configurations in which the cutting pattern causes ill-conditioning issues, preventing the use of iterative solvers.

Figure 1 showed an example in which the numerical problem is likely to be ill-conditioned. If the stiffness associated to the nodes outside the domain is small it leads to an ill-conditioning of the system of equations. This is because large variations of the solution at those pathological nodes do not affect the energy of the problem. That is, the global energy remains practically the same regardless of the solution at those nodes. In other words, the sensitivity of the energy to the variation of the solution at those nodes is small. Burman [19] found similar issues and addressed them adding an extra term, the ghost penalty, which stabilizes the solution of the pathological nodes by defining a polynomial expansion over a patch containing a sufficient number of elements into the physical domain Ω. However, this effective methodology requires to construct an additional operator build as the L_2 projection of the solution in the patch to a polynomial expansion, which is no standard in the FE framework. More recently, Badía *et. al.* [20] proposed a method in which they also add stiffness to those external nodes by generating aggregates. These aggregates are formed by the union of several elements surrounding an element with a small intersected area, thus forming a macro element that modifies the initial Cartesian structure of the mesh.

In this contribution, a new technique based on the use of recovered fields is introduced with the aim of, at least, solve the issue, common for the FDM, with the minimal interference on the Cartesian structure of the mesh and avoiding the construction of non-usual operators in FE. The proposed technique adds a term to (5) according to equation (6):

$$\mathscr{L}(\mathbf{w}^h, \boldsymbol{\chi}^h) = \mathscr{L}_0(\mathbf{w}^h, \boldsymbol{\chi}^h) - \frac{h}{k_1} \int_{\Gamma_D} \boldsymbol{\chi}^h \cdot (\boldsymbol{\lambda}^h + \mathbf{T}(\tilde{\mathbf{u}}^h)) \, \mathrm{d}\Gamma + \mathscr{S}(\mathbf{w}^h, \tilde{\mathbf{u}}^h), \tag{6}$$

where

$$\mathscr{S}(\mathbf{w}^h, \tilde{\mathbf{u}}^h) = \frac{k_2}{h^2} \int_{\hat{\Omega}^\star} \mathbf{w}^h \cdot (\mathbf{u}^h - \mathbf{S}(\tilde{\mathbf{u}}^h)) \, \mathrm{d}\Omega, \tag{7}$$

$k_1 = \kappa_1 E$ ($\kappa_1 > 0$) and $k_2 = \kappa_2 E$ ($\kappa_2 > 0$) are user-defined parameters, being E the Young's modulus. Note that $\hat{\Omega}^\star = \bigcup_{\mathrm{p}} \Omega_{\mathrm{p}} \cap \Omega^\star$, being Ω_{p} the domain of an element p containing at least one pathological node, i.e. a node associated to a small stiffness. The additional term, $\mathscr{S}(\mathbf{w}^h, \tilde{\mathbf{u}}^h)$, in equation (6) penalizes the "free" displacement of those pathological nodes. It introduces an artificial stiffness that is compensated with an artificial force as shown in Figure 3. In this term, the integration domain $\hat{\Omega}^\star$

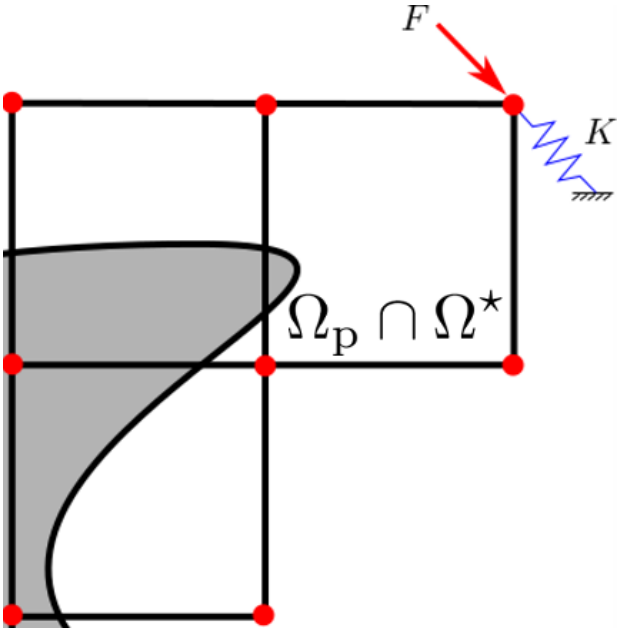

Figure 3: Scheme of an element subjected to ill-conditioning issues. Effect of the additional term.

corresponds to the volume (not the surface) of the elements containing pathological nodes. Thus, the integration domain now considers also the part of the element falling outside the problem domain. The operator $\mathbf{S}(\tilde{\mathbf{u}}^h)$ is a smoothed displacement field obtained as a postprocess of the FE solution $\tilde{\mathbf{u}}^h$. Further details of operator $\mathbf{S}$ are in Section 3.2. Note that one of the most important benefits of the method is that the additional term can be constructed as a lumped mass matrix, standard in the FE set.

Finally, the resulting saddle point reads as follows: find $(\mathbf{u}^h, \boldsymbol{\lambda}^h) \in V^h \times M^h$ such that:

$$\begin{aligned} a(\mathbf{u}^h, \mathbf{v}^h) + b(\boldsymbol{\lambda}^h, \mathbf{v}^h) + \frac{k_2}{h^2} \int_{\hat{\Omega}^\star} \mathbf{u}^h \cdot \mathbf{v}^h \, \mathrm{d}\Omega &= c(\mathbf{v}^h) + \frac{k_2}{h^2} \int_{\hat{\Omega}^\star} \mathbf{S}(\tilde{\mathbf{u}}^h) \cdot \mathbf{v}^h \, \mathrm{d}\Omega \\ b(\boldsymbol{\mu}^h, \mathbf{u}^h) - \frac{h}{k_1} \int_{\Gamma_D} \boldsymbol{\mu}^h \cdot \boldsymbol{\lambda}^h \, \mathrm{d}\Gamma &= b(\boldsymbol{\mu}^h, \bar{\mathbf{u}}) + \frac{h}{k_1} \int_{\Gamma_D} \boldsymbol{\mu}^h \cdot \mathbf{T}(\tilde{\mathbf{u}}^h) \, \mathrm{d}\Gamma, \end{aligned} \tag{8}$$

where $\mathbf{v}^h \in V^h$ and $\boldsymbol{\mu}^h \in M^h$ are the variations of the displacement and multiplier fields and $(\mathbf{u}^h, \boldsymbol{\lambda}^h)$ is the solution. Note that the variations of $\mathbf{S}(\tilde{\mathbf{u}}^h)$ and $\mathbf{T}(\tilde{\mathbf{u}}^h)$ are zero since they depend on the solution of previous Richardson's iterations but not on the current one. Additionally, the formulation can be simplified by eliminating the Lagrange multipliers. Since the Lagrange multiplier field lives in M^h which can be defined as a element-wise L_2 broken space, and following the method proposed in [28],

the second equation in (8) can be solved for each element:

$$\boldsymbol{\lambda}_e^h = \Pi^h \left(\frac{k_1}{h} \left(\mathbf{u}^h - \bar{\mathbf{u}} \right) - \mathbf{T}(\tilde{\mathbf{u}}^h) \right), \tag{9}$$

where Π^h is the L_2 projection onto M^h. Finally, substituting (9) in the first equation of (8) and operating as in [28] we obtain the following modified problem: find the displacement field $\mathbf{u}^h \in V^h$ such that:

$$a(\mathbf{u}^h, \mathbf{v}^h) + \frac{k_1}{h} \int_{\Gamma_D} \mathbf{u}^h \cdot \mathbf{v}^h \, \mathrm{d}\Gamma + \frac{k_2}{h^2} \int_{\hat{\Omega}^\star} \mathbf{u}^h \cdot \mathbf{v}^h \, \mathrm{d}\Omega = c(\mathbf{v}^h) + \frac{k_1}{h} \int_{\Gamma_D} \bar{\mathbf{u}}^h \cdot \mathbf{v}^h \, \mathrm{d}\Gamma + \int_{\Gamma_D} \mathbf{v}^h \cdot \mathbf{T}(\tilde{\mathbf{u}}^h) \, \mathrm{d}\Gamma + \frac{k_2}{h^2} \int_{\hat{\Omega}^\star} \mathbf{S}(\tilde{\mathbf{u}}^h) \cdot \mathbf{v}^h \, \mathrm{d}\Omega. \tag{10}$$

Note that the second and third terms of the left hand side in (10) are penalty terms with constants $\frac{k_1}{h}$ and $\frac{k_2}{h^2}$, respectively. The two last terms of the right hand side are a correction for the penalty term and a stabilization of the displacement field, respectively.

2.2 Iterative solver

Note that for solving problem (10) an iterative process is required since operators $\mathbf{T}$ and $\mathbf{S}$ depend on the solution. In this contribution the Richardson's method is implemented, considering $\mathbf{T} = \mathbf{S} = \mathbf{0}$ for the first iteration. Once the first iteration is obtained, the operators $\mathbf{T}$ and $\mathbf{S}$ are obtained as explained in Section 3, considering $\mathbf{T}(\tilde{\mathbf{u}}^h)$ and $\mathbf{S}(\tilde{\mathbf{u}}^h)$, being $\tilde{\mathbf{u}}^h$ the solution obtained in the previous Richardson's iteration. The convergence of this iterative process is demonstrated in Section 4.2.

This strategy for solving problem (10) results in an iterative solver. However, the system matrix remains constant in the proposed approach and only the right hand side is modified between the iterations. This considerably decreases the computational cost since it is possible to factorize the system matrix when direct solvers are used. Additionally, for large problems in which iterative solvers are needed (in this work the conjugate gradient method is considered), the preconditioner is only calculated once (the system matrix remains constant) and the solutions of the previous iterations can be used as an initial guess, speeding up the iterative solver. Note that the variations between the Richardson's iterations are small since they affect only a limited number of degrees of freedom

along the boundary. Additionally, the proposed method can be directly applied to solve problems with non-linear constitutive material behavior [11] without further modifications of terms in (10), only an external non-linear solver (i.e. Newton-Raphson) would be required as usual.

3 Recovery techniques

Zienkiewicz and Zhu developed an efficient and easy-to-implement error indicator in energy norm [29], based on the use of a recovered solution, of a higher quality than that of the raw FE solution, and built from this one. The accuracy of this error indicator depends, obviously, on the accuracy recovery technique used. Therefore, many recovery techniques have been developed during the last decades [30, 31, 32, 33, 34, 35], just to cite some. Among them, the Superconvergent Patch Recovery technique developed by Zienkiewicz and Zhu [30], which provides a robust, efficient and easy-to-implement error indicator can be highlighted. The recovery procedure used in this error indicator, also proposed by Zienkiewicz and Zhu, is at the base of the recovery techniques proposed in this contribution for the evaluation of the operators $\mathbf{S}$ and $\mathbf{T}$ used in Section 2 for the stabilization terms. In this Section, the proposed technique and the construction of the operators $\mathbf{T}$ and $\mathbf{S}$ introduced in Section 2 are shown.

The recovered field of an arbitrary vector field $\boldsymbol{\Upsilon}$ at each patch of elements i, $\hat{\boldsymbol{\Upsilon}}_i$, is obtained by minimizing the following functional:

$$\mathcal{F}_i(\hat{\boldsymbol{\Upsilon}}_i) = \int_{\hat{\Omega}_i} (\boldsymbol{\Upsilon}^h - \hat{\boldsymbol{\Upsilon}}_i)^2 \, \mathrm{d}\Omega, \tag{11}$$

where the field $\boldsymbol{\Upsilon}^h$ is a given FE interpolation of the field $\boldsymbol{\Upsilon}$ (i.e. displacements, strains, stresses, ...) and the field $\hat{\boldsymbol{\Upsilon}}_i$ is a polynomial expansion of a higher order than the FE interpolation (usually one order higher). A patch of elements $\hat{\Omega}_i$ consists of the elements attached to the node i, also called patch *assembly node*. Note that in the proposed approach the domain of the patch $\hat{\Omega}_i$ is not restricted to the physical domain Ω since it may include the part of the element falling outside the physical domain. Extra terms that improve the quality of the recovered field at each patch can also be added, depending on the needs such as static admissibility for the error estimator case, see for

instance [32, 36] or [37] for error upper bounds.

After obtaining the recovered field at each patch of elements, valid only in the patch surrounding the node i, the recovered field in the whole domain $\Omega^\star$ is obtained by using the Conjoint Polynomial Enhancement [31], which is nothing but the weighted sum of the contribution of each patch at a given position $\mathbf{x} \in \Omega^\star$:

$$\hat{\boldsymbol{\Upsilon}} = \sum_{j=1}^{Nvn} N(\mathbf{x})_j \hat{\boldsymbol{\Upsilon}}_j(\mathbf{x}), \tag{12}$$

where Nvn is the number of vertex nodes in an element and the weighting functions are the linear shape functions of the elements.

3.1 Operator T

The operator $\mathbf{T}$ is the projection of the recovered stress field to the boundary. That is, $\boldsymbol{\Upsilon}^h = \boldsymbol{\sigma}^h$, $\hat{\boldsymbol{\Upsilon}}_i = \hat{\boldsymbol{\sigma}}_i$ and $\hat{\boldsymbol{\Upsilon}} = \hat{\boldsymbol{\sigma}}$ in equation (11). Therefore:

$$\mathbf{T}(\mathbf{u}^h) = \hat{\boldsymbol{\sigma}} \cdot \mathbf{n}. \tag{13}$$

Note that operator $\mathbf{T}$ is only considered along the Dirichlet boundaries, see (5). This implies that the reconstruction of the stress field via the minimization of the functional (11) and the use of the Conjoint Polynomial Enhancement (12) is only required at patches cut by the Dirichlet boundary, which has a reduced computational cost.

3.2 Operator S

The operator $\mathbf{S}$ corresponds to the recovered displacement field obtained with the minimization of the functional (11). In this case $\boldsymbol{\Upsilon}^h = \mathbf{u}^h$ and $\hat{\boldsymbol{\Upsilon}}_i = \hat{\mathbf{u}}_i$ in equation (11). Therefore:

$$\mathbf{S}(\mathbf{u}^h) = \hat{\mathbf{u}}_i. \tag{14}$$

In this case, the operator $\mathbf{S}$ is only required along the part of the boundary influenced by pathological nodes. Hence, this procedure is computationally inexpensive. In contrast with operator $\mathbf{T}$, operator

S is evaluated at each node i (only the nodal value is retained), thus avoiding the use of the Conjoint Polynomial Enhancement (12).

4 Convergence study

In this Section, the different aspects of the convergence to the exact solution of the proposed approach are studied. First the *a priori* error estimates are analyzed to demonstrate the right convergence of all the operators involved. Then, the convergence of the iterative algorithm for the resolution of the problem is demonstrated and finally the improvement of the condition number thanks to the addition of the term $\mathscr{S}(\mathbf{v}^h, \mathbf{u}^h)$.

4.1 A priori error estimates

This Section shows that the additional term defined in equation (7) does not affect the convergence of the approximated solution to the exact solution as the mesh is uniformly refined, i.e. it has at least the same convergence rate than the strain energy [38], according to the following proposition.

Proposition 1. *The term defined in equation* (7) *vanishes with* h^{2p} *as the mesh is refined, being* p *the order of the polynomial interpolation, that is:*

$$\frac{\kappa_2 E}{h^2} \int_{\hat{\Omega}^\star} \mathbf{e}^h \cdot (\mathbf{e}^h - \mathbf{S}(\hat{\mathbf{e}}^h)) \, \mathrm{d}\Omega \approx \mathcal{O}(h^{2p}), \tag{15}$$

with $\mathbf{e}^h = \mathbf{u} - \mathbf{u}^h$*, being* $\mathbf{u}$ *the exact solution.*

Proof. The additional term can be bounded by using the Cauchy-Schwarz inequality:

$$\frac{\kappa_2 E}{h^2} \int_{\hat{\Omega}^\star} \mathbf{e}^h \cdot (\mathbf{e}^h - \mathbf{S}(\hat{\mathbf{e}}^h)) \, \mathrm{d}\Omega \lesssim h^{-2} \|\mathbf{e}^h\|_{L_2(\hat{\Omega}^\star)} \|\mathbf{e}^h - \mathbf{S}(\hat{\mathbf{e}}^h)\|_{L_2(\hat{\Omega}^\star)}, \tag{16}$$

with symbol $\lesssim$ indicating that the inequality holds up to a certain positive constant. Using the triangular inequality for the last norm in equation (16):

$$\|\mathbf{e}^h - \mathbf{S}(\hat{\mathbf{e}}^h)\|_{L_2(\hat{\Omega}^\star)} \lesssim \left(\|\mathbf{e}^h\|_{L_2(\hat{\Omega}^\star)} + \|\mathbf{S}(\hat{\mathbf{e}}^h)\|_{L_(\hat{\Omega}^\star)}\right). \tag{17}$$

Finally combining equation (17) in (16) is obtained that:

$$\frac{\kappa_2 E}{h^2}\int_{\hat{\Omega}^\star} \mathbf{e}^h \cdot (\mathbf{e}^h - \mathbf{S}(\hat{\mathbf{e}}^h))\,\mathrm{d}\Omega \lesssim h^{-2}\|\mathbf{e}^h\|_{L_2(\hat{\Omega}^\star)}\left(\|\mathbf{e}^h\|_{L_2(\hat{\Omega}^\star)} + \|\mathbf{S}(\hat{\mathbf{e}}^h)\|_{L_2(\hat{\Omega}^\star)}\right). \tag{18}$$

To check the convergence, attention must be paid to the term $\|\mathbf{S}(\hat{\mathbf{e}}^h)\|_{L_2(\hat{\Omega}^\star)}$. This term is built as the L_2-projection to a local and richer space, i.e. a higher-order polynomial space, thus the convergence of $\|\mathbf{S}(\hat{\mathbf{e}}^h)\|_{L_2(\hat{\Omega}^\star)}$ is the same as the convergence of $\|\mathbf{e}^h\|_{L_2(\hat{\Omega}^\star)}$ due to the orthogonality of (11), then:

$$\frac{\kappa_2 E}{h^2}\int_{\hat{\Omega}^\star} \mathbf{e}^h \cdot (\mathbf{e}^h - \mathbf{S}(\hat{\mathbf{e}}^h))\,\mathrm{d}\Omega \lesssim h^{-2}\|\mathbf{e}^h\|^2_{L_2(\hat{\Omega}^\star)} \approx \mathcal{O}(h^{2p}). \tag{19}$$

□

4.2 Iterative solver convergence

As observed in equation (10), the RHS of the system of equations depends on the solution of the same system. Then, the Richardson's method is used for solving the linear system of equations.

In matrix notation, equation (10) can be expressed as follows:

$$\mathbf{A}\mathbf{d}^i = \mathbf{c} + \mathbf{B}\mathbf{d}^{i-1}, \tag{20}$$

being $\mathbf{d}^i$ the solution at iteration i. The matrix $\mathbf{A}$ is obtained from:

$$a(\mathbf{v}^h, \mathbf{v}^h) + \frac{\kappa_1 E}{h}\int_{\Gamma_D} \mathbf{v}^h \cdot \mathbf{v}^h\,\mathrm{d}\Gamma + \frac{\kappa_2 E}{h^2}\int_{\hat{\Omega}^\star} \mathbf{v}^h \cdot \mathbf{v}^h\,\mathrm{d}\Omega, \tag{21}$$

and matrix $\mathbf{B}$ is obtained from

$$\int_{\Gamma_D} \mathbf{v}^h \cdot \mathbf{T}(\hat{\mathbf{v}}^h)\, \mathrm{d}\Gamma + \frac{\kappa_2 E}{h^2} \int_{\hat{\Omega}^\star} \mathbf{v}^h \cdot \mathbf{S}(\hat{\mathbf{v}}^h)\, \mathrm{d}\Omega, \tag{22}$$

where $\hat{\mathbf{v}}^h$ is the solution of iteration $i-1$, which in practice will never be assembled. Richardson's method is proved to converge if the spectral radius of the matrix $\mathbf{A}^{-1}\mathbf{B}$ is smaller than one.

Proposition 2. *The spectral radius of* $\mathbf{A}^{-1}\mathbf{B}$ *is smaller than 1, that is* $\rho(\mathbf{A}^{-1}\mathbf{B}) \leq 1$*, for appropriate values of* κ_1 *and* κ_2*, independent of* h*.*

Proof. In this case, any eigenvalue λ satisfies:

$$\mathbf{A}^{-1}\mathbf{B}\mathbf{d} = \lambda \mathbf{d}. \tag{23}$$

Pre-multiplying both sides by $\mathbf{d}^T\mathbf{A}$ we obtain:

$$\mathbf{d}^T\mathbf{B}\mathbf{d} = \lambda \mathbf{d}^T\mathbf{A}\mathbf{d}. \tag{24}$$

It can be observed that the LHS of equation (24) corresponds to the stabilization terms for a given field $\mathbf{v}^h$, then:

$$\mathbf{d}^T\mathbf{B}\mathbf{d} = \int_{\Gamma_D} \mathbf{v}^h \cdot \mathbf{T}(\mathbf{v}^h)\, \mathrm{d}\Gamma + \frac{k_2}{h^2} \int_{\hat{\Omega}^\star} \mathbf{v}^h \cdot \mathbf{S}(\mathbf{v}^h)\, \mathrm{d}\Omega. \tag{25}$$

In the same way:

$$\mathbf{d}^T\mathbf{A}\mathbf{d} = a(\mathbf{v}^h, \mathbf{v}^h) + \frac{\kappa_1}{h} \int_{\Gamma_D} \mathbf{v}^h \cdot \mathbf{v}^h\, \mathrm{d}\Gamma + \frac{k_2}{h^2} \int_{\hat{\Omega}^\star} \mathbf{v}^h \cdot \mathbf{v}^h\, \mathrm{d}\Omega. \tag{26}$$

Then, after some algebra and applying the Cauchy-Schwarz inequality, the following expression is obtained:

$$\lambda \mathbf{d}^T \mathbf{A} \mathbf{d} = \mathbf{d}^T \mathbf{B} \mathbf{d} \leq \|\mathbf{v}^h\|_{L^2(\Gamma_D)} \|\mathbf{T}(\mathbf{v}^h)\|_{L^2(\Gamma_D)} + \frac{k_2}{h^2} \|\mathbf{v}^h\|_{L^2(\Omega^\star)} \|\mathbf{S}(\mathbf{v^h})\|_{L^2(\Omega^\star)}. \tag{27}$$

According to [11], the term $\|\mathbf{T}(\mathbf{v}^h)\|_{L^2(\Gamma_D)}$ can be bounded by the energy norm of the problem, thus the first term of the RHS in equation (27) can be bounded by the energy norm as follows:

$$\|\mathbf{v}^h\|_{L^2(\Gamma_D)} \|\mathbf{T}(\mathbf{v}^h)\|_{L^2(\Gamma_D)} \leq \|\mathbf{v}^h\|_{L^2(\Gamma_D)} \left(\frac{C_E C_p C_r}{h} \right)^{\frac{1}{2}} \|\mathbf{v}^h\|_E, \tag{28}$$

where $\|\mathbf{v}^h\|_E$ stands for the energy norm, $C_E = \frac{E}{1+2\nu}$, C_p stands for the Poincaré inequality and C_r is the constant relating a recovered field with the FE field into a bounded domain, i.e. $\|\mathbf{T}(\mathbf{v}^h)\|^2_{L^2(\cdot)} \leq C_r \|\boldsymbol{\sigma}(\mathbf{v}^h)\|^2_{L^2(\cdot)}$. It is important to note that C_E, C_p and C_r are independent of the mesh size. Further details on these constants can be found in [11].

Finally, applying the triangular inequality ($2xy \leq \frac{x^2}{2} + \frac{y^2}{2}$) the following equation is obtained:

$$\|\mathbf{v}^h\|_{L^2(\Gamma_D)} \|\mathbf{T}(\mathbf{v}^h)\|_{L^2(\Gamma_D)} \leq \|\mathbf{v}^h\|^2_E + \frac{C_E C_p C_r}{4h} \|\mathbf{v}^h\|^2_{L^2(\Gamma_D)}. \tag{29}$$

On the other hand, it is also necessary to bound the second term of the RHS in equation (27). Considering the relation between a recovered solution and the corresponding FE solution is $\|\hat{\boldsymbol{\Upsilon}}^h_i\|^2_{L^2(\cdot)} \leq \|\boldsymbol{\Upsilon}^h\|^2_{L^2(\cdot)}$, due to the orthogonality of the operator (11), the following expression is written:

$$\|\mathbf{v}^h\|_{L^2(\hat{\Omega}^\star)} \|\mathbf{S}(\mathbf{v}^h)\|_{L^2(\hat{\Omega}^\star)} \leq \|\mathbf{v}^h\|^2_{L^2(\hat{\Omega}^\star)}. \tag{30}$$

Note that equation (30) holds for an appropriate selection of the patches for evaluating operator $\mathbf{S}$ such that $\oplus_i \hat{\Omega}_i = \hat{\Omega}^\star$. Finally, substituting (29) and (30) in (27) the next equation is found:

$$\lambda \mathbf{d}^T \mathbf{A} \mathbf{d} \leq \|\mathbf{v}^h\|^2_E + \frac{C_E C_p C_r}{4h} \|\mathbf{v}^h\|^2_{L^2(\Gamma_D)} + \frac{k_2}{h^2} \|\mathbf{v}^h\|^2_{L^2(\hat{\Omega}^\star)}. \tag{31}$$

Considering that:

$$\mathbf{d}^T\mathbf{A}\mathbf{d} = \|\mathbf{v}^h\|_E^2 + \frac{k_1}{h}\|\mathbf{v}^h\|_{L^2(\Gamma_D)}^2 + \frac{k_2}{h^2}\|\mathbf{v}^h\|_{L^2(\hat{\Omega}^\star)}, \tag{32}$$

it suffices in taking $k_1 > \frac{C_E C_p C_r}{4h}$ for any value of k_2 to ensure that $\lambda < 1$.

□

4.3 Improvement of the condition number

In the standard, conforming, Finite Element setting, the condition number grows with h^{-2}. This Section shows that the proposed method provides a condition number that grows as in the standard FE case.

Proposition 3. *The condition number of the system of equations resulting from equation* (10) *grows with* h^{-2}.

Proof. The condition number is the ratio between the smaller and higher eigenvalues λ_{min} and λ_{max}, $\kappa = \frac{\lambda_{max}}{\lambda_{min}}$. In this case, it is necessary to proof *i)* $\lambda_{min} > 0$ independently of h and *ii)* λ_{max} is proportional to h^{-2}.

i) $\lambda_{min} > 0$ *independently of* h

For this part of the proof it is necessary to check the coercivity, i.e. if there exists $C_1 > 0$, independent of h, such that:

$$C_1\|\mathbf{v}^h\|_{L^2(K)}^2 \leq h^2\left(a_{K\cap\Omega}(\mathbf{v^h},\mathbf{v^h}) + \frac{k_1}{h}\int_{\partial K\cap\Gamma_D}\mathbf{v}^h\cdot\mathbf{v}^h\,\mathrm{d}\Gamma, + \frac{k_2}{h^2}\int_K \mathbf{v}^h\cdot\mathbf{v}^h\,\mathrm{d}\Omega\right) \tag{33}$$

where $K \in \Omega^\star$ represents a single finite element of size h. Equation (33) follows from the mesh-dependent norm definition, see lemma 4.5.3 in [39]. The previous expression indicates that the displacement field is bounded by the energy, that is, any displacement field should produce a certain level of energy in the problem. In this part of the proof, the stabilization term proposed plays an

important role since it avoids the free movement of the pathological nodes without generating any energy in the system. Under the cgFEM framework, the effective domain falling into one element $(K \cap \Omega)$ does not depend on h but on how the geometry intersects the mesh. Therefore, the effective domain is bounded above by K and bounded below by $\emptyset$, i.e. $\emptyset \subseteq K \cap \Omega \subseteq K$, then, the terms:

$$a_{K\cap\Omega}(\mathbf{v^h}, \mathbf{v^h}), \qquad \text{and} \qquad \frac{k_1}{h}\int_{\partial K\cap\Gamma_D} \mathbf{v}^h \cdot \mathbf{v}^h \, \mathrm{d}\Gamma \tag{34}$$

can eventually tend to zero. That would prevent from fulfilling the coercivity property. However, making use of the last term in equation (33), since it does not depend on the physical domain Ω (i.e. it does not depend on how the mesh and geometry intersect), in the eventual case that the two first terms are close to zero, it will be possible to find a constant $C_1 > 0$ which ensures the coercivity. Since the problem is coercive, the norm of the minimum eigenvalue is higher than 0, $\lambda_{min} > 0$.

ii) $\lambda_{max} \propto h^{-2}$

On the other hand, according to the lemma 4.5.3 in [39] and adding the contributions of all the elements, we obtain:

$$a(\mathbf{v}^h, \mathbf{v}^h) + \frac{k_1}{h}\int_{\Gamma_D} \mathbf{v}^h \cdot \mathbf{v}^h \, \mathrm{d}\Gamma + \frac{k_2 E}{h^2}\int_{\hat{\Omega}^\star} \mathbf{v}^h \cdot \mathbf{v}^h \, \mathrm{d}\Omega \leq C_2 h^{-2} \|\mathbf{v}^h\|^2_{L^2(\Omega^\star)}. \tag{35}$$

Previous equations follow from the mesh-dependent norm definition that relates the energy norm with the norm of the solution. In this case, a bounded displacement filed will always produce a bounded energy value (bounded values of the gradients of the solution), following the continuity of the operators. According to the definition of spectral radius, it is known that $\lambda_{max} \propto C_2 h^{-2}$. Finally, combining the two results: $\lambda_{min} > 0$ and $\lambda_{max} \propto C_2 h^{-2}$ the next equation is found:

$$\kappa = \frac{\lambda_{max}}{\lambda_{min}} \propto h^{-2}. \tag{36}$$

□

5 Solution algorithm

In each iteration of the Richardson's method, for a given field $\tilde{\mathbf{u}}^h$, the system of equations obtained from (10) must be solved. It is assumed that at Richardson's iteration i, $\mathbf{u}^h_{i-1}$ is known, then the procedure can be summarized as follows:

1. Evaluate the stabilization terms for $\mathbf{u}^h_{i-1}$, $\mathbf{S}(\mathbf{u}^h_{i-1})$ and $\mathbf{T}(\mathbf{u}^h_{i-1})$ with equations (14) and (13), respectively.
2. Solve problem (10) and obtain $\mathbf{u}^h_i$.
3. Evaluate $\epsilon^R_i = ||\mathbf{u}^h_i - \mathbf{u}^h_{i-1}||_2$.
4. If $\epsilon^R_i < Tol$ stop the iterations, else go to step 1.

This Richardson's method is initialized with $\mathbf{u}^h_0 = \mathbf{0}$. Note that step 2 implies to solve several times a system of equations with the same system matrix. This allows us to factorize for speeding up the computations for direct solvers. For a large system of equations, when iterative solvers are required, the iterative method uses the solution of the previous Richardson's iteration and the tolerance of the iterative solver (ϵ^I_i) decreases proportionally to ϵ^R_i, i.e. $\epsilon^I_i \propto \epsilon^R_i$. This nested procedure for both iterative methods increases the performance of the solver.

6 Numerical results

In this Section, a series of numerical tests are carried out to check the improvements on the condition number and in the solution when using the proposed approach and, therefore, in the performance of the cgFEM.

6.1 Problem 1. Cylinder under internal pressure

This numerical example consists of a 3D model of a cylinder under internal pressure. The analytical solution for the plane strain case is known (37). Using a cylindrical reference system (r, θ, z), centred in the hole, the stress field is described by the following expressions:

$$\begin{cases} \sigma_{rr}(r,\theta,z) = \dfrac{Pr_i^2}{r_e^2 - r_i^2}\left(1 + \dfrac{r_e^2}{r^2}\right), \\ \sigma_{\theta\theta}(t,\theta,z) = \dfrac{Pr_i^2}{r_e^2 - r_i^2}\left(1 - \dfrac{r_e^2}{r^2}\right), \\ \sigma_{zz}(t,\theta,z) = \dfrac{Pr_i^2}{r_e^2 - r_i^2} \end{cases} \tag{37}$$

being $P = 10$ the internal pressure, $r_i = 5$ the internal radius and $r_e = 20$ the external radius. The Poisson's ratio is $\nu = 0.3$ and the Young's modulus is $E = 1000$. The 3D model and an example of the FE mesh (Mesh Level 5, i.e. 2^5 divisions per direction in the octree-mesh) provided by the cgFEM are shown in Figure 4. Symmetry boundary conditions are considered at planes $x = 0$ and $z = 0$. Also symmetry boundary conditions at planes $y = 0$ and $y = 20$ are considered to simulate the plane strain state. For this problem Q8 linear elements are considered. The corresponding von Mises stress field for this problem solved with Mesh Level 5 is shown in Figure 5.

The first study consists in the analysis of the convergence of the iterative solver, considering two situations: with and without the new stabilization term (7) introduced in this publication. The iterative solver is the PCG solver implemented in Matlab® configured with a null initialization solution. A sequence of 6 uniformly refined meshes, ranging from Mesh Level 2 to Mesh Level 7, have been considered for this problem. Table 1 shows the values of the condition numbers and the degrees of freedom of each Mesh Level. The results show that when no stabilization is used, the condition number takes high values and it grows with the Mesh Level. These values of the condition number could strongly affect the convergence of the iterative solver. On the other hand, when the stabilization is used ($\kappa_2 = 10^{-3}$ or $\kappa_2 = 10^{-4}$), the condition number takes considerably lower values.

Figure 6a shows that the number of iterations required when the proposed stabilization term is not

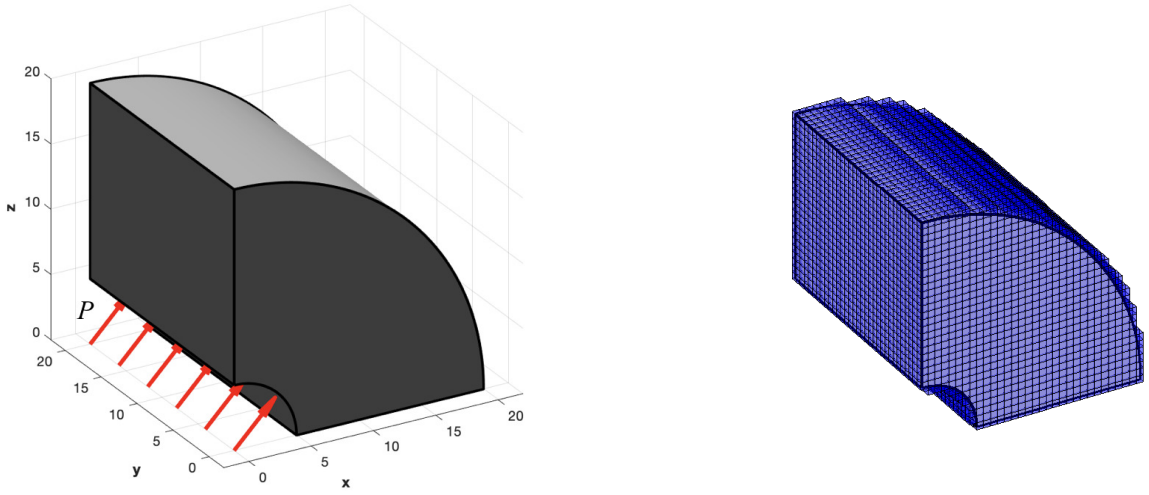

Figure 4: Cylinder under internal pressure. Domain and mesh example with Mesh Level 5. Symmetry boundary conditions on planes $x = 0$, $y = 0$, $z = 0$ and $y = 20$.

Table 1: Cylinder under internal pressure. Condition number of the system of equations.

Mesh Level	DoF	Cond. num. (No stabilized)	Cond. num. ($\kappa_2 = 10^{-3}$)	Cond. num. ($\kappa_2 = 10^{-4}$)
2	360	$2.87 \cdot 10^5$	$7.57 \cdot 10^4$	$2.27 \cdot 10^5$
3	1,890	$1.94 \cdot 10^{21}$	$6.87 \cdot 10^4$	$6.87 \cdot 10^5$
4	11,526	$7.55 \cdot 10^{20}$	$8.45 \cdot 10^4$	$6.87 \cdot 10^5$
5	69,750	$6.78 \cdot 10^{18}$	$8.58 \cdot 10^4$	$7.53 \cdot 10^5$

used is considerably higher, explaining the higher computational cost. Moreover, Figure 6b shows that the relative exact error in energy norm during the uniform refinement process for several stabilized cases and the non-stabilized case is mainly the same. It can be observed that the convergence remains unadulterated keeping a convergence rate of $\frac{1}{3}$, the theoretical convergence rate for linear elements. These results numerically confirm the theoretical proof of Section 4.1 in which the stabilization term properly vanishes with the mesh size at the appropriate rate. It should be mentioned that the number of Richardson's iterations is influenced by the value of κ_2: higher values of κ_2 will require more Richardson's iterations. For this example, for Mesh Level 6, when no stabilization is used, the number of Richardson's iterations is 5, 6 for $\kappa_2 = 10^{-4}$ and 12 for $\kappa_2 = 10^{-3}$. Each

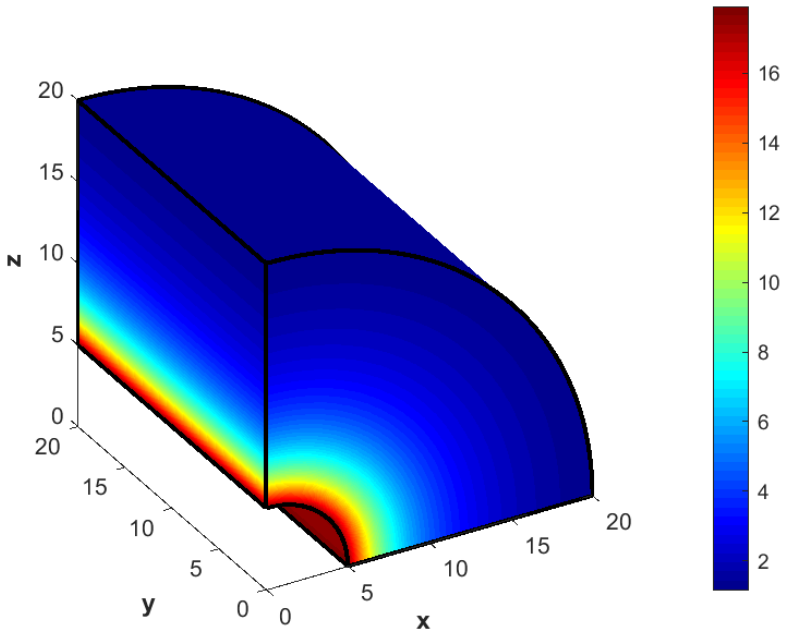

Figure 5: Cylinder under internal pressure. Von Mises stress field.

Richardson's iteration implies solving the system of equations only once, but, for the subsequent iterations, since an accurate initial solution is already available, the solution time is considerably reduced. In any case, the reduction of the solution time when the stabilization is used compensates for the increment of Richardson's iterations.

Regarding the FE results, the displacement field at elements containing a pathological node is not strongly influenced by solution at these nodes since they are far from the problem domain and the interpolation decreases the influence of the pathological nodes on the solution. However, for the case of the stress field, the influence of the solution at the pathological nodes is not attenuated since the derivatives of the shape functions are used. Therefore the quality of the stress field at those elements is strongly related to the use of the stabilization technique. For this problem, the results of the relative maximum difference (infinite norm) between the exact von Mises stress field at the external boundary and the evaluated von Mises stress field are shown in Table 2. It can be appreciated that, when the stabilization is used, the results are similar and an improvement up to 21.9% is achieved, with a clear increasing trend with the mesh refinement for this numerical test, compared to the

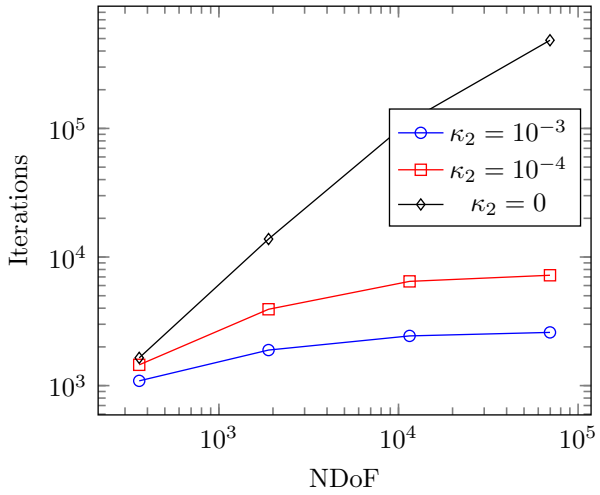

(a) Convergence of the iterative solver. Number of iterations required for a relative tolerance of 10^{-12}.

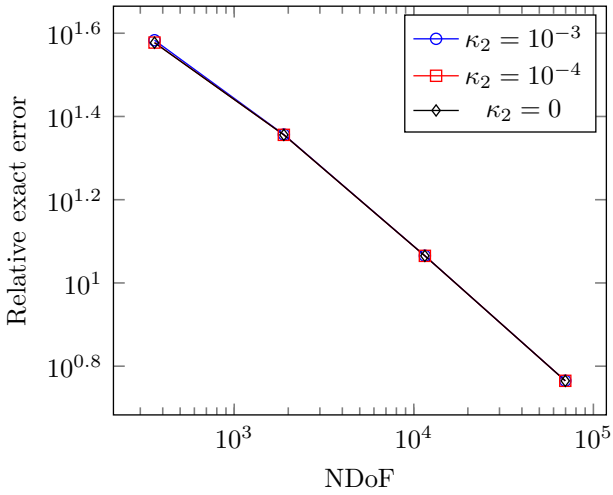

(b) Convergence of the solution, considering the relative exact error in energy norm.

Figure 6: Cylinder under internal pressure. Convergence analysis. $\kappa_2 = 0$ means no stabilization.

non-stabilized test.

Additionally, it must be taken into account that the condition number is strongly affected by the intersection pattern when the stabilization method is not used. This fact can be seen in the following example in which the intersection pattern has been deliberately modified, by slightly modifying the mesh limits, to observe this effect. For this test, three analyses with different configurations yielding three different intersection patterns with Mesh Level 4 are carried out, as shown in Figure 7. The configuration shown in Figure 7a corresponds to the configuration used for the previous tests. The results in Table 3 show that when no stabilization is considered, the condition number strongly depends on the intersection pattern for very similar meshes. On the other hand, when the stabilization procedure is used, the condition number is almost independent of the intersection pattern.

Table 2: Cylinder under internal pressure. Infinite norm of the relative error between the exact Von Mises stress field and the FE stress field at the external boundary and relative improvement ($\Delta(\%)$) compared to $\kappa_2 = 0$.

Mesh Level	DoF	$\kappa_2 = 0$	$\kappa_2 = 10^{-3}$	$\Delta(\%)_{\kappa_2=10^{-3}}$	$\kappa_2 = 10^{-4}$	$\Delta(\%)_{\kappa_2=10^{-4}}$
2	360	$2.45 \cdot 10^{-1}$	$2.39 \cdot 10^{-1}$	2.51	$2.45 \cdot 10^{-1}$	0
3	1,890	$1.83 \cdot 10^{-1}$	$1.61 \cdot 10^{-1}$	13.7	$1.81 \cdot 10^{-1}$	1.1
4	11,526	$8.4 \cdot 10^{-2}$	$7.86 \cdot 10^{-2}$	6.87	$7.65 \cdot 10^{-2}$	9.8
5	69,750	$3.9 \cdot 10^{-2}$	$3.36 \cdot 10^{-2}$	16.1	$3.66 \cdot 10^{-2}$	6.56
6	512,766	$1.95 \cdot 10^{-2}$	$1.6 \cdot 10^{-2}$	21.9	$1.62 \cdot 10^{-2}$	20.4
7	3,788,127	–	$7.56 \cdot 10^{-3}$	–	$8.12 \cdot 10^{-3}$	–

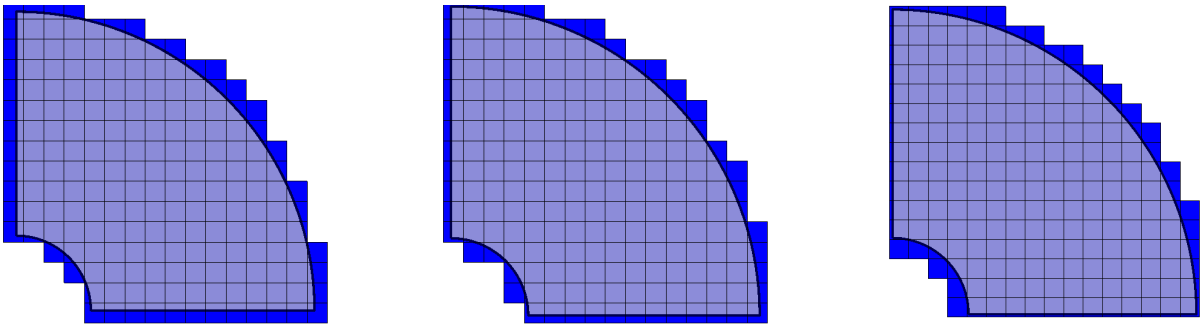

(a) Mesh configuration 1. (b) Mesh configuration 2. (c) Mesh configuration 3.

Figure 7: Cylinder under internal pressure. Mesh Level 4. The mesh size is configured with different percentages of clearance with the size of the body.

Table 3: Cylinder under internal pressure. Condition number for three different mesh configurations with Mesh Level 4.

Configuration Mesh	$\kappa_2 = 0$	$\kappa_2 = 10^{-3}$	$\kappa_2 = 10^{-4}$
1	$7.55 \cdot 10^{20}$	$4.45 \cdot 10^{4}$	$6.778 \cdot 10^{5}$
2	$2.79 \cdot 10^{7}$	$6.91 \cdot 10^{4}$	$6.53 \cdot 10^{5}$
3	$6.63 \cdot 10^{9}$	$8.69 \cdot 10^{4}$	$8.64 \cdot 10^{5}$

6.2 Problem 2. Threaded screw

This second numerical problem consists in a more challenging 3D geometry simulating a simplified model of a threaded screw. Figure 8a shows the geometry and the boundary conditions. In this case, homogeneous Dirichlet boundary conditions are applied to the top face of the screw (blue triangles at $x = 10$) while a normal pressure $P = 1 \cdot 10^8 Pa$ is applied over the red area. An isotropic linear elastic material model is considered with Young's modulus $E = 116 \cdot 10^9 Pa$ and Poisson's ratio $\nu = 0.3$. Figure 8b shows a sample of the coarsest mesh used to solve the problem. This mesh was created with 12794 h-adapted trilinear elements. The h-adaptive process was driven by the geometrical details in this case. Finally, Figure 9 shows a representation of the von Mises stress field considering the mesh shown in Figure 8b.

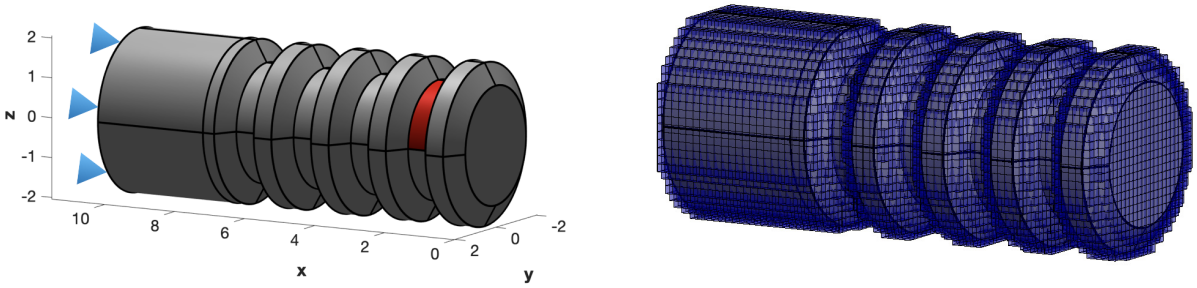

(a) Geometrical model. Blue triangles represent the surface over which the Dirichlet boundary conditions are applied while the red surface represents where the Neumann boundary conditions are applied.

(b) Sample of the coarsest mesh used for solving the problem.

Figure 8: Threaded screw model.

Two simulations, one with the mesh represented in Figure 8b and another with a more refined mesh, were carried out in this problem. In this case, an incomplete Cholesky's factorization was used as a preconditioner to solve the problem using the PCG algorithm implemented in Matlab®. The results regarding the number of iterations of the iterative solver and the condition number are shown in Table 4. As it can be observed, there is a substantial reduction of the condition number and also a reduction in the number of iterations, even if the preconditioner is used.

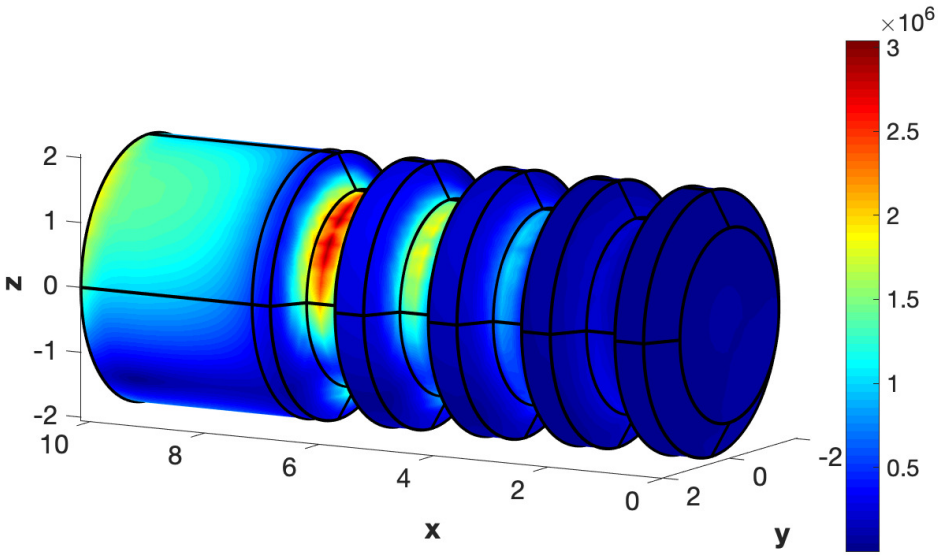

Figure 9: Screw. Von Mises stress field in Pa.

Table 4: Screw. Condition number and number of iterations of the PCG iterative solver, using the incomplete Cholesky's factorization.

NDoFs	$\kappa_2 = 0$		$\kappa_2 = 10^{-3}$	
	Condition Number	Iterations	Condition Number	Iterations
43470	$8.25 \cdot 10^{23}$	719	$2.51 \cdot 10^{6}$	614
266859	$6.89 \cdot 10^{37}$	1212	$2.72 \cdot 10^{6}$	976

7 Conclusions

This contribution tries to address the common issue of the FDM, particularly the cgFEM, when the mesh-geometry cutting pattern may yield an ill-conditioned system of equations. The proposed approach stabilizes the formulation by adding an extra term to the weak form of the problem.

Making use of Richardson's method used for the stabilization of the Lagrange multipliers field for imposing the Dirichlet boundary conditions, this new term is naturally included during the solving loop. Therefore, its evaluation is inexpensive since only requires a post-process of the solution along the boundary while preserving the Cartesian structure of the cgFEM framework.

The results show independence of the condition number regardless of the mesh-geometry intersection, yielding a speed-up of the solving process while preserving the consistency of the formulation.

Acknowledgments

The authors wish to thank the Spanish "Ministerio de Economía y Competitividad", the "Generalitat Valenciana" and the "Universitat Politècnica de València" for their financial support received through the projects DPI2017-89816-R, Prometeo 2016/007 and the FPI2015 program, respectively.

References

[1] Burman E, Hansbo P. Fictitious domain finite element methods using cut elements: I. A stabilized Lagrange multiplier method. Computer Methods in Applied Mechanics and Engineering. 2010;199(41-44):2680–2686. Available from: http://linkinghub.elsevier.com/retrieve/pii/S004578251000160X.

[2] Ruiz-Girons E, Sarrate J. Generation of structured hexahedral meshes in volumes with holes. Finite Elements in Analysis and Design. 2010 oct;46(10):792–804. Available from: https://www.sciencedirect.com/science/article/pii/S0168874X10000715?via{%}3Dihubhttp://linkinghub.elsevier.com/retrieve/pii/S0168874X10000715.

[3] Geuzaine C, Remacle JF. Gmsh: a three-dimensional finite element mesh generator with built-in pre-and post-processing facilities. International Journal for Numerical Methods in Engineering 79(11). 2009;0:1309–1331. Available from: http://gmsh.info/doc/preprints/gmsh{_}paper{_}preprint.pdf.

[4] Parvizian J, Düster A, Rank E. Finite cell method. Computational Mechanics. 2007 sep;41(1):121–133. Available from: http://link.springer.com/10.1007/s00466-007-0173-y.

[5] Düster A, Parvizian J, Yang Z, Rank E. The finite cell method for three-dimensional problems of solid mechanics. Computer Methods in Applied Mechanics and Engineering. 2008 aug;197(45-48):3768–3782. Available from: http://www.sciencedirect.com/science/article/pii/S0045782508001163.

[6] Nadal E, Ródenas JJ, Albelda J, Tur M, Tarancón JE, Fuenmayor FJ. Efficient Finite Element Methodology Based on Cartesian Grids: Application to Structural Shape Optimization. Abstract and Applied Analysis. 2013;p. 1–19. Available from: http://www.hindawi.com/journals/aaa/2013/953786/.

[7] Nadal E, Ródenas JJ, Sánchez-Orgaz EM, López-Real S, Martí-Pellicer J. Sobre la utilización de códigos de elementos finitos basados en mallados cartesianos en optimización estructural.

Revista Internacional de Métodos Numéricos para Cálculo y Diseño en Ingeniería. 2014 jul;30(3):155–165. Available from: http://www.sciencedirect.com/science/article/pii/S021313151300059Xhttp://dx.doi.org/10.1016/j.rimni.2013.04.009https://www.scipedia.com/public/Nadal{_}et{_}al{_}2013a.

[8] Giovannelli L, Ródenas JJ, Navarro-Jiménez JM, Tur M. Direct medical image-based Finite Element modelling for patient-specific simulation of future implants. Finite Elements in Analysis and Design. 2017 nov;136:37–57. Available from: https://www.sciencedirect.com/science/article/pii/S0168874X1630498X.

[9] Schillinger D, Ruess M. The Finite Cell Method: A Review in the Context of Higher-Order Structural Analysis of CAD and Image-Based Geometric Models. Archives of Computational Methods in Engineering. 2015;22(3):391–455. Available from: http://dx.doi.org/10.1007/s11831-014-9115-y.

[10] Burman E, Claus S, Hansbo P, Larson MG, Massing A. CutFEM: Discretizing geometry and partial differential equations. International Journal for Numerical Methods in Engineering. 2015 nov;104(7):472–501. Available from: http://doi.wiley.com/10.1002/nme.4823.

[11] Tur M, Albelda J, Marco O, Ródenas JJ. Stabilized method of imposing Dirichlet boundary conditions using a recovered stress field. Computer Methods in Applied Mechanics and Engineering. 2015 aug;296:352–375. Available from: http://www.sciencedirect.com/science/article/pii/S0045782515002467.

[12] Tur M, Albelda J, Nadal E, Ródenas JJ. Imposing Dirichlet boundary conditions in hierarchical Cartesian meshes by means of stabilized Lagrange multipliers. International Journal for Numerical Methods in Engineering. 2014 may;98(6):399–417. Available from: http://onlinelibrary.wiley.com/doi/10.1002/nme.4629/abstracthttp://doi.wiley.com/10.1002/nme.4629.

[13] de Prenter F, Verhoosel CV, van Zwieten GJ, van Brummelen EH. Condition number analysis and preconditioning of the finite cell method. Computer Methods in Applied Mechanics and Engineering. 2017 apr;316:297–327. Available from: http://dx.doi.org/10.1016/j.cma.2016.07.006https://linkinghub.elsevier.com/retrieve/pii/S0045782516307277.

[14] Berger-Vergiat L, Waisman H, Hiriyur B, Tuminaro R, Keyes D. Inexact Schwarz-algebraic multigrid preconditioners for crack problems modeled by extended finite element methods. International Journal for Numerical Methods in Engineering. 2012 apr;90(3):311–328. Available from: http://doi.wiley.com/10.1002/nme.3318.

[15] Menk A, Bordas SPA. A robust preconditioning technique for the extended finite element method. International Journal for Numerical Methods in Engineering. 2011 apr;85(13):1609–1632. Available from: http://doi.wiley.com/10.1002/nme.3032.

[16] Dauge M, Düster A, Rank E. Theoretical and Numerical Investigation of the Finite Cell Method. Journal of Scientific Computing. 2015;65(3):1039–1064. Available from: http://dx.doi.org/10.1007/s10915-015-9997-3.

[17] Elfverson D, Larson MG, Larsson K. CutIGA with basis function removal. Advanced Modeling and Simulation in Engineering Sciences. 2018 dec;5(1):6. Available from: https://doi.org/10.1186/s40323-018-0099-2https://amses-journal.springeropen.com/articles/10.1186/s40323-018-0099-2.

[18] Verhoosel CV, van Zwieten GJ, van Rietbergen B, de Borst R. Image-based goal-oriented adaptive isogeometric analysis with application to the micro-mechanical modeling of trabecular bone. Computer Methods in Applied Mechanics and Engineering. 2015;284:138–164. Available from: http://dx.doi.org/10.1016/j.cma.2014.07.009.

[19] Burman E. La pénalisation fantôme. Comptes Rendus Mathematique. 2010;348(21-22):1217–1220. Available from: http://dx.doi.org/10.1016/j.crma.2010.10.006.

[20] Badia S, Verdugo F, Martín AF. The aggregated unfitted finite element method for elliptic problems. 2017 sep;(September 2017). Available from: http://arxiv.org/abs/1709.09122http://dx.doi.org/10.1016/j.cma.2018.03.022.

[21] Jomo JN, de Prenter F, Elhaddad M, D'Angella D, Verhoosel CV, Kollmannsberger S, et al. Robust and parallel scalable iterative solutions for large-scale finite cell analyses. Finite Elements in Analysis and Design. 2019;163(June):14–30. Available from: https://doi.org/10.1016/j.finel.2019.01.009.

[22] Béchet E, Moës N, Wohlmuth B, Béchet É, Moës N, Wohlmuth B. A stable Lagrange multiplier space for stiff interface conditions within the extended finite element method. International Journal for Numerical Methods in Engineering. 2009 may;78(8):931–954. Available from: http://doi.wiley.com/10.1002/nme.2515http://www3.interscience.wiley.com/journal/121578755/abstract.

[23] Hautefeuille M, Annavarapu C, Dolbow JE. Robust imposition of Dirichlet boundary conditions on embedded surfaces. International Journal for Numerical Methods in Engineering. 2012 apr;90(1):40–64. Available from: http://doi.wiley.com/10.1002/nme.3306.

[24] Hansbo P, Lovadina C, Perugia I, Sangalli G. A Lagrange multiplier method for the finite element solution of elliptic interface problems using non-matching meshes. Numerische Mathematik. 2005 mar;100(1):91–115. Available from: http://link.springer.com/10.1007/s00211-005-0587-4.

[25] Burman E, Hansbo P. Fictitious domain finite element methods using cut elements: II. A stabilized Nitsche method. Applied Numerical Mathematics. 2012;62(4):328–341. Available from: http://dx.doi.org/10.1016/j.apnum.2011.01.008.

[26] Gerstenberger A, Wall W. An eXtended Finite Element Method/Lagrange multiplier based approach for fluid-structure interaction. Computer Methods in Applied Mechanics and Engineering. 2008;197(19-20):1699–1714. Available from: http://linkinghub.elsevier.com/retrieve/pii/S0045782507002915.

[27] Axelsson O. Iterative Solution Methods. 1994;.

[28] Stenberg R. On some techniques for approximating boundary conditions in the finite element method. Journal of Computational and Applied Mathematics. 1995;63(1-3):139–148.

[29] Zienkiewicz OC, Zhu JZ. A simple error estimator and adaptive procedure for practical engineering analysis. International Journal for Numerical Methods in Engineering. 1987;24(2):337–357. Available from: http://onlinelibrary.wiley.com/doi/10.1002/nme.1620240206/abstract.

[30] Zienkiewicz OC, Zhu JZ. The superconvergent patch recovery and a posteriori error estimates. Part 1: The recovery technique. International Journal for Numerical Methods in Engineering. 1992;33(7):1331–1364. Available from: http://www3.interscience.wiley.com/journal/110549860/abstracthttp://www3.interscience.wiley.com/journal/110549866/abstract.

[31] Blacker T, Belytschko T. Superconvergent patch recovery with equilibrium and conjoint interpolant enhancements. International Journal for Numerical Methods in Engineering. 1994;37(3):517–536. Available from: isi:A1994MT59900008.

[32] Díez P, Ródenas JJ, Zienkiewicz OC, Pedro D, Díez P, Ródenas JJ, et al. Equilibrated patch recovery error estimates : simple and accurate upper bounds of the error. International Journal for Numerical Methods in Engineering. 2007;69(August 200610):2075–2098. Available from: http://onlinelibrary.wiley.com/doi/10.1002/nme.1837/abstract.

[33] Xiao QZ, Karihaloo BL. Statically admissible stress recovery using the moving least squares technique. In: Topping BHV, Soares CAM, editors. Congress in Computational Structures Technology. Stirling, Scotland: Saxe-Coburg Publications; 2004. p. 111–138.

[34] Ródenas JJ, Tur M, Fuenmayor FJ, Vercher A. Improvement of the superconvergent patch recovery technique by the use of constraint equations: the SPR-C technique. International Journal for Numerical Methods in Engineering. 2007;70(6):705–727.

[35] Zhang Z. A posteriori error estimates on irregular grids based on gradient recovery. Advances in Computational Mathematics. 2001;15:363–374. Available from: http://www.springerlink.com/index/cywwd0tm6c17tem8.pdf.

[36] González-Estrada OA, Nadal E, Ródenas JJ, Kerfriden P, Bordas SPa, Fuenmayor FJ. Mesh adaptivity driven by goal-oriented locally equilibrated superconvergent patch recovery. Computational Mechanics. 2013 oct;53(5):957–976. Available from: http://link.springer.com/10.1007/s00466-013-0942-8.

[37] Nadal E, Díez P, Ródenas JJ, Tur M, Fuenmayor FJ. A recovery-explicit error estimator in energy norm for linear elasticity. Computer Methods in Applied Mechanics and Engineering. 2015;287:172–190.

[38] Alan DJ. The Finite Element Method; 1980.

[39] Brenner SC, Scott LR. Mathematical Theory of Finite Element Methods. Marsde JE, Sirovich L, Golubisky M, Jäger W, John F, editors. Springer Berlin Heidelberg; 1994.